AD-A172 130 ELASTIC WAVE SCATTERING BY SURFACE-BREAKING PLANAR AND NON-PLANAR CRACKS..(U) COLORADO UNIV AT BOULDER DEPT OF MECHANICAL ENGINEERING A H SHAH ET AL. AUG 86 1/1

UNCLASSIFIED CUMER-86-6 N00014-86-K-0280 F/G 14/2 NL

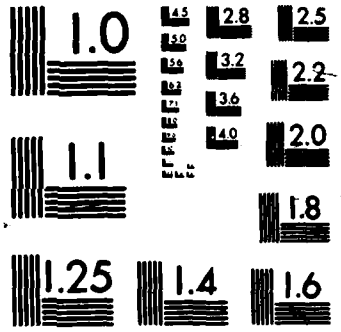
1.0
1.1
1.25
1.4
1.6
1.8
2.0
2.2
2.5
2.8
3.2
3.6
4.0
4.5
5.0
5.6

(1)

ELASTIC WAVE SCATTERING BY SURFACE-BREAKING PLANAR AND NON-PLANAR CRACKS

A. H. Shah and Y. F. Chin[1]

S. K. Datta[2]

CUMER-86-6 August 1986

Contract N00014-86-K-0280

[1]Department of Civil Engineering
University of Manitoba, Winnipeg, Canada R3T 2N2

[2]Department of Mechanical Engineering and CIRES
University of Colorado, Boulder, Colorado
Fellow, ASME

ULTRASONIC SCATTERING AND NONDESTRUCTIVE EVALUATION OF DEFECTS

SUBHENDU K. DATTA[1], ARVIND H. SHAH[2]

(1) Department of Mechanical Engineering and Cooperative Institute for Research in Environmental Sciences, University of Colorado, Boulder, CO 80309, U.S.A.; (2) Department of Civil Engineering, University of Manitoba, Winnipeg, Canada R3T 2N2

INTRODUCTION

At present ultrasonic techniques for characterizing defects are being explored vigorously at various research centers around the world. Currently, the ultrasonic approach to defect sizing and characterization is beginning to find great favor for in- or out-of-service use. For a recent review of practical ultrasonic nondestructive evaluation the reader is referred to Silk (1). Because of recent advances in experimental ultrasonic technology, increasing demands are being put on quantitative theoretical modeling of scattering of ultrasonic (elastic) waves by cracks, cavities and other material inhomogeneities in an elastic medium. With a view to obtain detailed information about signals scattered from complex defects various analytical and numerical techniques have emerged. In this article we present a combined finite element and eigenfunction expansion technique for solving scattering problems involving multiple scattering as well as complex geometries. Numerical results obtained by this method are compared with recent experimental results. In the following we first summarize the theoretical treatment. Then we present the finite element and eigenfunction expansion technique (FEEET). Numerical and experimental results are presented next. Although the results presented here are for homogeneous materials, the method can readily be extended to composite materials.

GOVERNING EQUATIONS AND METHODS OF SOLUTION

For the development of the main concepts behind solution techniques for scattering in an elastic medium we will assume that the medium is infinite in extent, is homogeneous, isotropic, and linearly elastic with Lamé elastic constants λ, μ, and density, ρ. An infinite solid right cylinder with material constants λ_1, μ_1, and ρ_1 is assumed to be embedded in the infinite medium. For convenience it will be further assumed that the problem is two-dimensional (plane strain) in planes perpendicular to the axis of the cylinder. Let xy-plane be a plane perpendicular to the axis and let the boundary of the intersection of this plane with the cylinder be C.

The equation of motion in the elastic medium is given by

$$\nabla \cdot \tau + \rho\omega^2 u = 0 \tag{1}$$

where $u(x,y)e^{-i\omega t}$ is the displacement of a point of the medium, τ is the associated stress tensor, and ω is the circular frequency. τ is related to the displacement gradients by the relation

$$\tau = \lambda I(\nabla \cdot u) + \mu(\nabla u + u\nabla) \tag{2}$$

where I is the identity tensor.

Now the scattering problem is to find the solution u of (1) such that

$$u = u^{(0)} + u^{(s)}, (x,y) \quad \text{outside} \quad C \tag{3}$$

where $u^{(0)}$ is the incident field that satisfies (1) in the absence of the inclusion, and $u^{(s)}$ is the scattered field that also satisfies (1) outside C and the radiation condition as $r = \sqrt{x^2+y^2} \to \infty$. Furthermore, if the field inside C is denoted by u_1, then u_1 satisfies (1) and (2) with λ, μ, and ρ replaced by λ_1, μ_1, and ρ_1, respectively. The boundary conditions on C are,

$$\begin{aligned} u &= u_1 \quad \text{on} \quad C \\ n \cdot \tau &= n \cdot \tau_1 \quad \text{on} \quad C \end{aligned} \tag{4}$$

Here it has been assumed that the cylinder is perfectly bonded with the surrounding medium and n is an outward unit normal to C. The solution, $u^{(s)}$, has a surface integral representation (See, Varatharajulu and Pao (2)),

$$u^{(0)}(r) + \int_C \{u'[n' \cdot \overleftrightarrow{\sum}(r|r')] - n' \cdot \tau' \cdot G\} ds' = \begin{cases} u(r); r \quad \text{outside} \quad C \\ 0; r \quad \text{inside} \quad C \end{cases} \tag{5}$$

Here $\overleftrightarrow{\sum}$ is related to the Green's tensor G by the equation

$$\overleftrightarrow{\sum} = \lambda I \nabla \cdot G + \mu(\nabla G + G\nabla) \tag{6}$$

The primes indicate that the quantities are evaluated at points r' on C. The Green's tensor G satisfies the equation

$$\nabla \cdot \overleftrightarrow{\sum}(r|r') + \rho\omega^2 G(r|r') = -I\delta(r - r') \tag{7}$$

Note that if r approaches C then the left-hand side of (5) gives $\frac{1}{2}u(r)$. Equation (5) is the basis of the various boundary integral approaches that have been developed to solve scattering problems involving arbitrary geometry of C. The common difficulty encountered when using these methods is in treating multiple scatterers, scatterers with sharp edges, and scatterers in inhomogeneous or anisotropic regions. For these reasons we have developed a hybrid method that combines the advantages of the finite element method with those of the integral representation or of the eigenfunction representation. The hybrid combined finite element and eigenfunction representation has been used by us in solving

several scattering problems that involve non-planar cracks, multiple cavities, and cracks in a bounded medium.

In this approach Equation (5) is solved by expanding u in a set of basis vector functions that satisfy (1). For the two-dimensional problem under consideration these are (Varatharajulu and Pao (2)), using plane polar coordinates r, θ,

$$\phi_n^\sigma(r) = \begin{cases} \nabla[\epsilon_n^{\frac{1}{2}} H_n(k_1 r) cosn\theta] & ; \quad \sigma = 1 \\ \nabla[\epsilon_n^{\frac{1}{2}} H_n(k_1 r) sinn\theta] & ; \quad \sigma = 2 \end{cases} \tag{8}$$

and

$$\psi_n^\sigma(r) = \begin{cases} \nabla \wedge [e_z \epsilon_n^{\frac{1}{2}} H_n(k_2 r) cosn\theta] & ; \quad \sigma = 1 \\ \nabla \wedge [e_z \epsilon_n^{\frac{1}{2}} H_n(k_2 r) sinn\theta] & ; \quad \sigma = 2 \end{cases} \tag{9}$$

where $\epsilon_0 = 1$, and $\epsilon_n = 2 (n > 0)$; $H_n(kr)$ is the Hankel function of the first kind. The basis functions (8) and (9) are used to represent the scattered field $u^{(s)}$. On the other hand, the incident field $u^{(0)}$ is represented in terms of $Re\psi_n^\sigma$, where Re denotes the real part of H_n, which is J_n. The quantities k_2, k_1 are the longitudinal and shear wave numbers,

$$k_1 = \omega / c_1 \quad , \quad k_2 = \omega / c_2 \tag{10}$$

c_1, c_2 being the longitudinal and shear wave speeds outside C.

Thus one writes

$$u^{(0)}(r) = \sum_{n,\sigma} [A_n^\sigma \phi_n^\sigma + B_n^\sigma Re\psi_n^\sigma] \tag{11}$$

$$u^{(s)}(r) = \sum_{n,\sigma} [\alpha_n^\sigma \phi_n^\sigma + \beta_n^\sigma \psi_n^\sigma] \tag{12}$$

Representations (11) and (12) are valid outside the scatterer(s). So they are valid also outside an imaginary boundary B circumscribing the scatterer(s).

The field inside this boundary is represented by finite elements. The two solutions are then matched by requiring the continuity of displacements and tractions across B. It has been shown that this finite element and eigenfunction expansion technique (FEEET) is quite versatile in solving scattering by cracks or multiple cavities in bounded media as well as structure-medium interaction problems (Shah, Wong and Datta, (3); Abduljabbar, Datta and Shah, (4); Shah, Wong and Datta, (5); Datta, Wong and Shah, (6); Wong, Shah and Datta, (7)). In the following we describe the method and present numerical results. We also present some experimental results.

The combined finite element representation inside B and the integral representation (5) outside B was used in (8) to study dynamic amplification of surface displacements.

HYBRID FINITE-ELEMENT AND EIGENFUNCTION TECHNIQUE

For the two-dimensional problem considered in this paper, the solution for the displacement u can be divided into two parts: the anti-plane motion (SH) in which $u_x = u_y = 0$, $u_z \neq 0$, and the in-plane motion in which $u_z = 0$, $u_x \neq 0$, $u_y \neq 0$. The SH wave scattering in semi-infinite media and thick plates was studied by Datta, Shah and Fortunko (9), Abduljabbar, Datta and Shah (4), and Abduljabbar (10).

Consider a surface-breaking crack of length D making an angle α with the x-axis (See, Fig. 1). Note that the crack may be embedded in a material that has different material properties from the surrounding homogeneous, isotropic elastic medium. Let a plane SH wave be given by

$$u_z^{(i)} \begin{cases} \equiv \omega^i(x,y)e^{i\omega t} \\ = \omega_0 e^{i\epsilon(\bar{x}\sin\gamma - \bar{y}\cos\gamma) - i\omega t} \end{cases} \tag{13}$$

be incident from infinity. Here $\epsilon = k_2 D, \bar{x} = x/D$, and $\bar{y} = y/D$. Figure 1 shows the geometry. The incident field given by (13) will be reflected from the free surface so that the total field incident on the crack is

$$u_z^{(0)} = 2\omega_0 \cos(\epsilon\bar{y}\cos\gamma)e^{i\epsilon\bar{x}\sin\gamma} = \omega^{(0)} \tag{14}$$

where we have dropped the time factor $e^{-i\omega t}$. The scattered field will be denoted by $u_z^{(s)} \equiv \omega^{(s)}$.

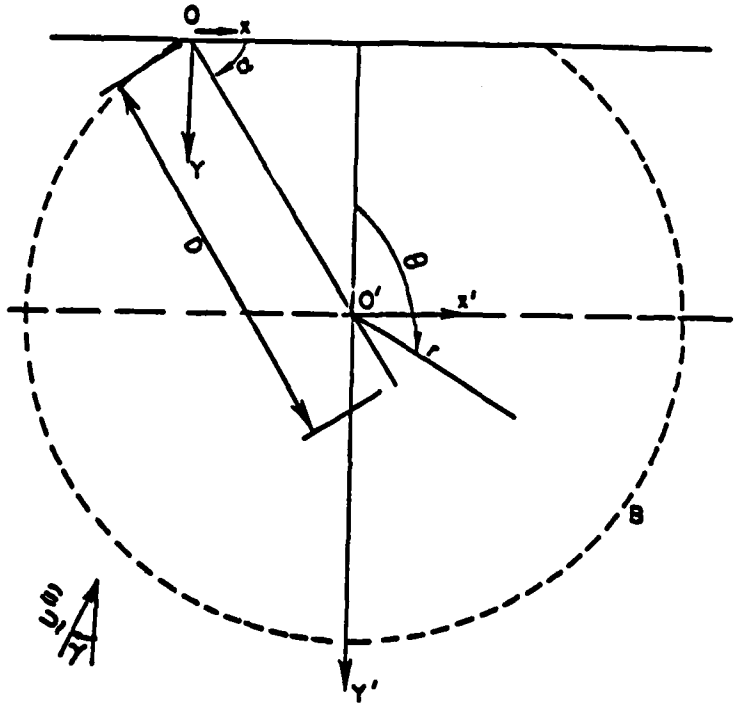

FIGURE 1. Geometry of a surface-breaking crack.

The solution $\omega^{(s)}$ outside an imaginary surface B enclosing the crack can be expanded as,

$$\omega^{(s)} = \sum_{n=1}^{\infty} A_n cosn\theta' H_n(k_2 r') \tag{15}$$

where r', θ' are defined as

$$r' = (x^2 + y^2)^{\frac{1}{2}} \quad , \quad r' cos\theta' = x$$

The surface B can be chosen as a semi-circle of radius $r' = R_B$. Note that $\omega^{(s)}$ satisfies the stress-free boundary condition on $y = 0$.

The region interior to B (including B) will be divided into finite elements. Thus the displacement in the domain of an element can be written in the form

$$\omega_i = \sum_{i=1}^{M} L_i(\xi, \eta) W_i \tag{16}$$

where M is the number of nodes in the element, $\omega_i (i = 1, .., M)$ are the nodal displacements and L_i are the shape functions.

The variational formulation requires the minimization of the functional

$$f = U - \frac{1}{2}\rho_e \omega^2 \int\int \omega^T \bar{\omega} dx dy - \frac{1}{2}\sum_{i=1}^{M}(p_i \bar{W}_i + \bar{p}_i W_i) \tag{17}$$

where $p_i (i = 1, ..., M)$ are the nodal forces and the integral is over the area of the element. U is the strain energy given by

$$U = \frac{1}{2}\mu_e \int\int \{\frac{\delta\omega}{\delta x}\frac{\delta\bar{\omega}}{\delta x} + \frac{\delta\omega}{\delta y}\frac{\delta\bar{\omega}}{\delta y}\} dx dy \tag{18}$$

In the above overbar indicates complex conjugation and subscript e denotes element property. Minimization of f leads to the equation

$$[K]\{W\} = \{p\} \tag{19}$$

where [K] is an MXM matrix whose elements are given by

$$K_{ij} = \int_{-1}^{1}\int_{-1}^{1} [\{(\alpha \frac{\partial L_i}{\partial \xi}\frac{\partial L_j}{\partial \xi}) + \gamma(\frac{\partial L_i}{\partial \xi}\frac{\partial L_j}{\partial \eta} + \frac{\partial L_i}{\partial \eta}\frac{\partial L_j}{\partial \xi}) +$$

$$\beta(\frac{\partial L_i}{\partial \eta}\frac{\partial L_j}{\partial \eta})\}\frac{1}{|J|} - \rho_e \omega^2 L_i L_j |J|] d\xi d\eta \tag{20}$$

$$\alpha = \mu_e\{(\frac{\partial y}{\partial \eta})^2 + (\frac{\partial x}{\partial \eta})^2\}$$

$$\beta = \mu_e\{(\frac{\partial y}{\partial \xi})^2 + (\frac{\partial x}{\partial \xi})^2\}$$

$$\gamma = -\mu_e(\frac{\partial y}{\partial \xi}\frac{\partial y}{\partial \eta} + \frac{\partial x}{\partial \xi}\frac{\partial x}{\partial \eta})$$

$$|J| = (\frac{\partial x}{\partial \xi}\frac{\partial y}{\partial \eta} - \frac{\partial x}{\partial \eta}\frac{\partial y}{\partial \xi})$$

For the crack problem in the absence of body forces under consideration the interior nodal forces are zero. So assembling the element equations we get the global equation

$$\begin{bmatrix} S_{II} & S_{IB} \\ S_{IB} & S_{BB} \end{bmatrix} \begin{Bmatrix} W_I \\ W_B \end{Bmatrix} = \begin{Bmatrix} 0 \\ p_B \end{Bmatrix} \tag{21}$$

where subscripts I and B denote internal and boundary nodes, respectively. Here $\{p_B\}$ denotes the column matrix of interaction forces at B between the regions interior and exterior to B. Then we require that

$$\{W_B\} = \{\omega_B^{(0)} + \omega_B^{(s)}\}$$

$$\{\tilde{p}_B\} = \{p_B\} \tag{22}$$

where $\tilde{p}_B$ is a weighted average traction derived from $\omega = \omega^{(0)} + \omega^{(s)}$. Details of this can be found in Datta and Shah (11). Using equation (20) in conjunction with (15) and (21), one obtains equations for the determination of the coefficients A_n and the nodal displacements W_I and W_B. Once A_n's are known, then the scattered displacement field can be calculated. Figure 2 shows the amplitude of the scattered field (normalized with respect to the amplitude of the incident field) on $y = 0$ for large k_2x when $\alpha = 90°$. The incident field direction is parallel to the x-axis ($\gamma = 90°$). Also shown on this figure are experimental results obtained on a number of calibration specimens using electromagnetic acoustic transducers (EMAT). For details of the experimental set-up, reference may be made to Datta, Shah and Fortunko (9).

The method described above can be used also to analyze scattering in a thick plate. Then the representation (15) for the scattered field is replaced by

$$\omega^{(s)} = \sum_{n=0}^{\infty} B_n cos\beta_n y e^{ik_n x} \quad , \quad x\rangle 0$$

$$= \sum_{n=0}^{\infty} C_n cos\beta_n y e^{-ik_n x} \quad , \quad x\langle 0 \tag{23}$$

where $\beta_n = n\pi/h$, $k_n = (k_2^2 - \beta_n^2)^{\frac{1}{2}}$, h being the thickness of the plate. The fictitious boundary B is now replaced by vertical lines at $x = -x_L$ and $x = x_R$ that join the horizontal surfaces $y = 0$ and $y = h$. Figure 3 shows backscattered amplitude due to a

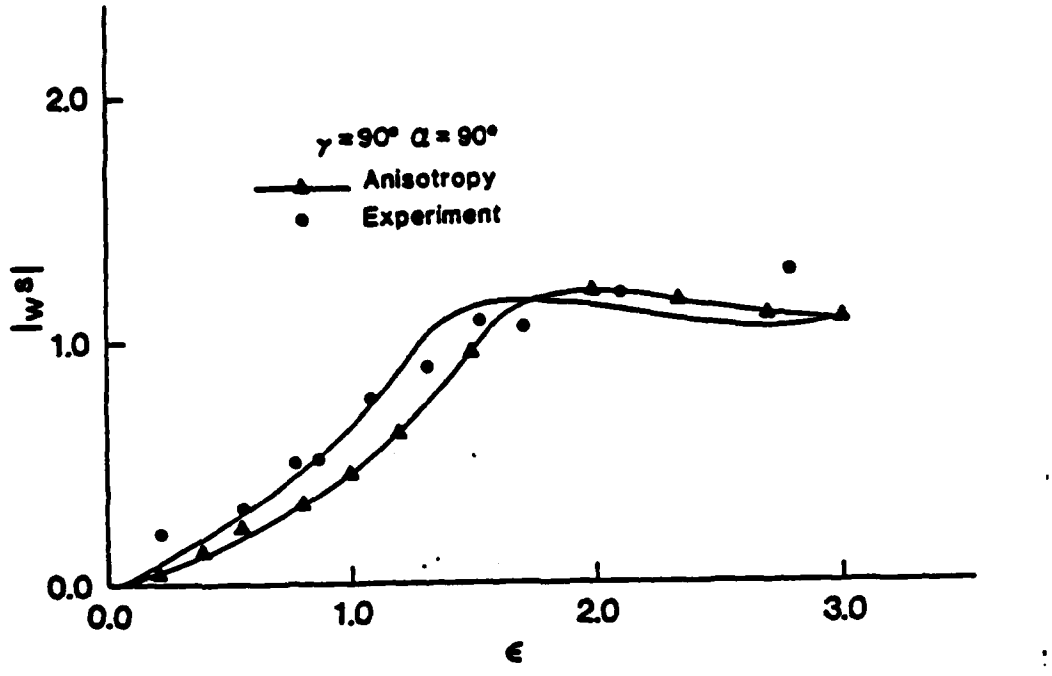

FIGURE 2. Scattered SH wave far-field amplitude for a normal surface-breaking crack. Grazing incidence.

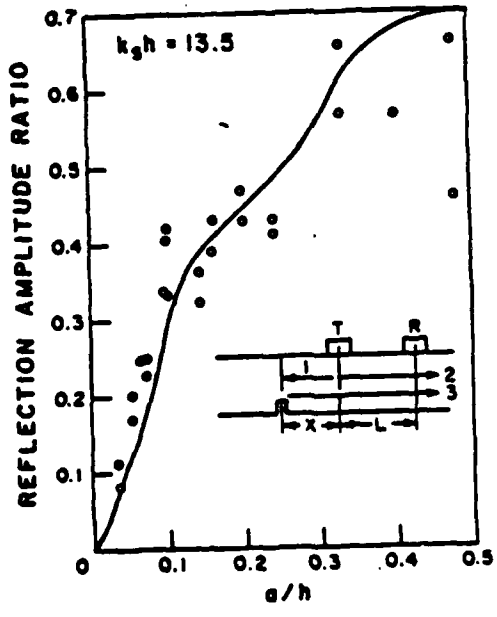

FIGURE 3. Scattered SH wave amplitude in a thick plate. a is the length of the crack, h the thickness of the plate and $k_s = \omega/c_2$.

normal surface crack ($\alpha = 90°$). Also shown in the figure are the experimentally-measured values. In the experiment both the transmitters and receivers were sensitive to $n = 0$ and 1 modes only.

Scattering by buried canted crack ($\alpha \neq 90°$) in a thick plate has also been analyzed using the above technique. Experiments have also been performed. Details of the analytical and experimental procedures are discussed in (12). Figure 4 shows the experimental configuration and the geometry of the crack. In this case several plate modes (n=0, ..., 4) were generated and received by the transducers. Figures 5 and 6 show the reflected and transmitted transient signals at different receiver locations for the same transmitter location. It is seen that for certain locations the agreement between theory and experiment is quite good. However, there are other locations at which there is significant discrepancy. There may be several reasons for this: finite transducer size, crack lengths in the experimental configuration not being exactly the same as that assumed for analysis, and, perhaps, the most important fact being that the cracks in the experiments were surface-breaking.

We now present some results for the plane strain case. In this case the scattered field $u^{(s)}$ can be represented in the form (12) with

$$\phi_n^\sigma = \nabla\phi_n^P + \nabla\phi_n^S$$
$$\psi_n^\sigma = \nabla \wedge (\psi_n^S e_z) + \nabla \wedge (\psi_n^P e_z) \qquad (24)$$

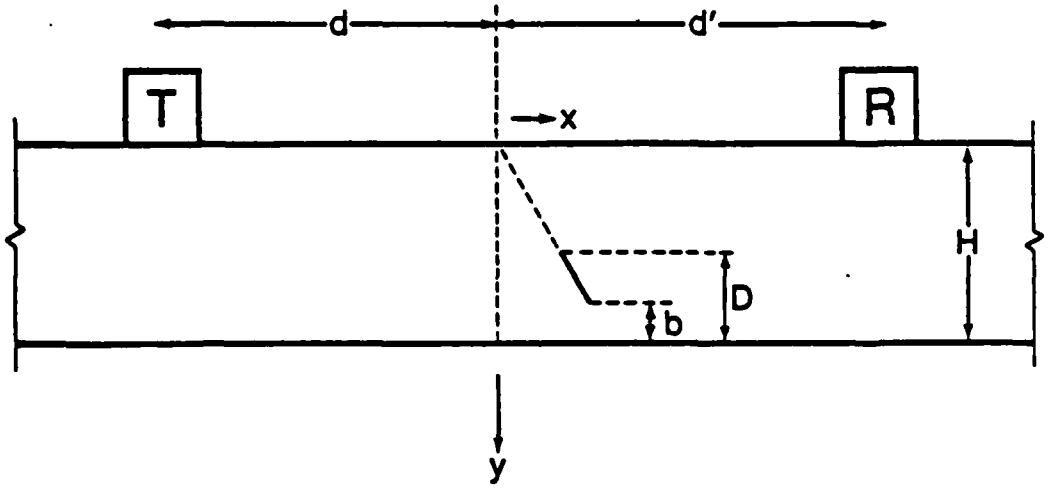

FIGURE 4. Experimental configuration.

For convenience, ϕ_n^σ and ψ_n^σ are now defined as $\phi_n e^{in\theta}$, $\psi_n e^{in\theta}$, and the sum in (12) is over n only, but from $-\infty$ to ∞. The functions ϕ_n^P, ψ_n^P, ϕ_n^S, and ψ_n^S are such that $u^{(s)}$ satisfies the stress-free boundary condition on $y = 0$. Their expressions can be found in Datta and El-Akily (13). The boundary B in Figure 1 can be chosen to intersect the free surface as shown, if the scatterer is very close to $y = 0$, or it can be wholly within the half-space if the scatterer is embedded deep in the half-space. The latter was the case discussed by Shah, Wong and Datta (5), and Wong, Shah and Datta (6). More recently, scattering from surface-breaking cracks has been discussed by Shah, Chin and Datta (14).

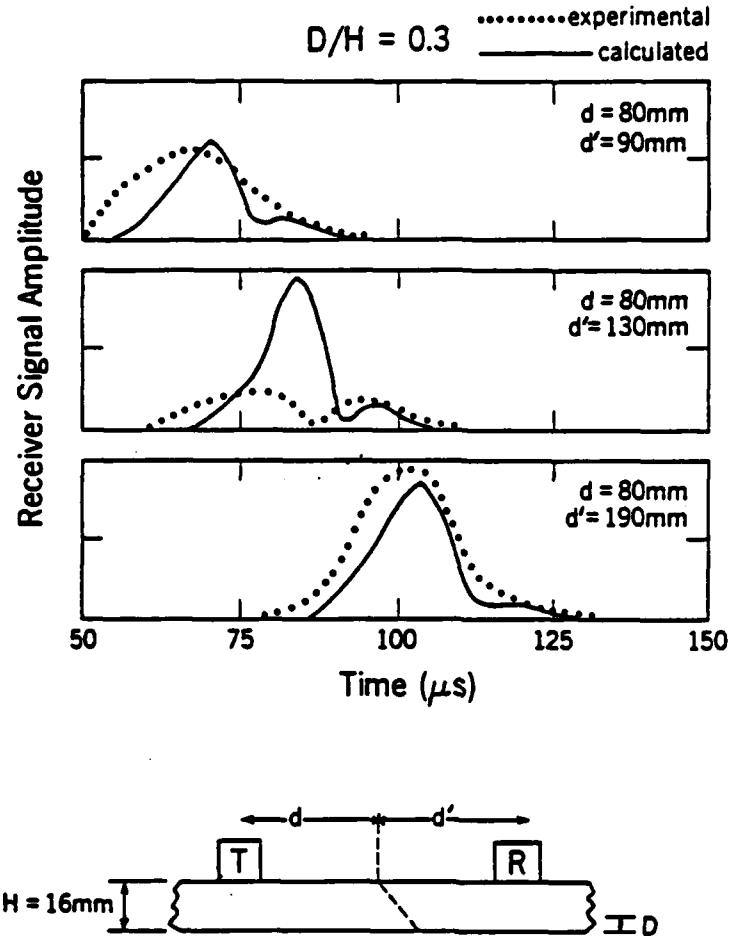

FIGURE 5. Transmitted pulse for a 30° canted buried crack.

In Figure 7 we show the results of normalized scattered vertical surface displacements due to a buried circular cavity. Results of experiments and earlier asymptotic calculations are also shown. Figure 8 shows the corresponding results for a buried circular elastic inclusion. It is seen that in both cases there is very good agreement between theory and experiment. Finally, Figures 9-11 show the results for surface-breaking straight and branched cracks for an incident Rayleigh wave propagating in the x-direction.

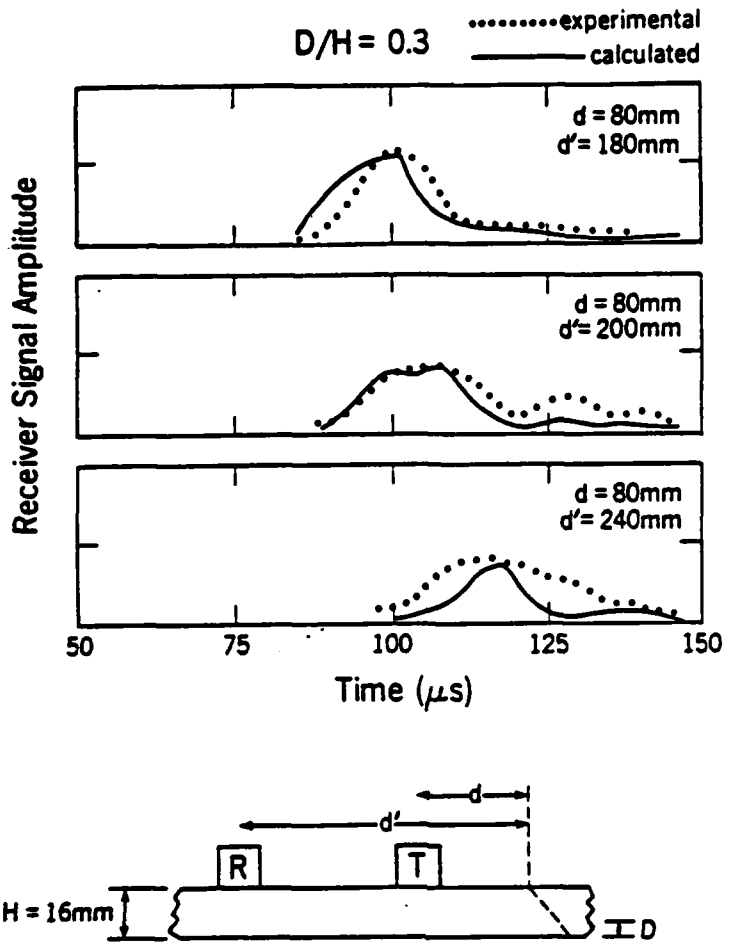

FIGURE 6. Reflected pulse for a 30° canted buried crack.

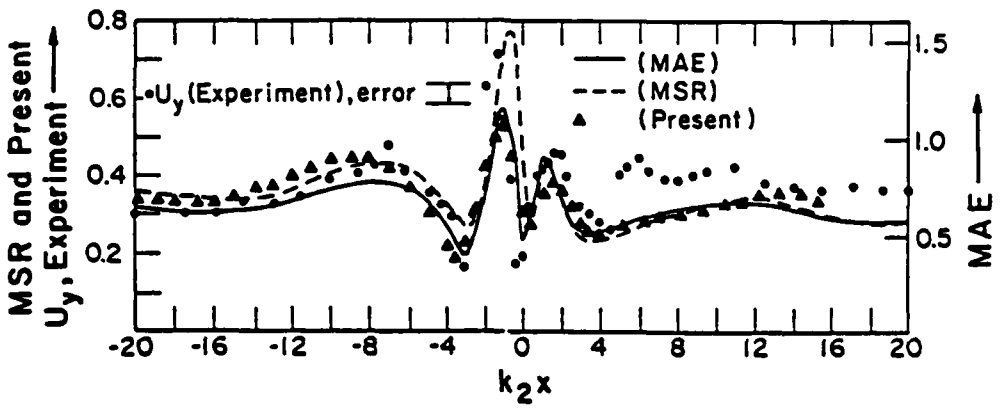

FIGURE 7. Scattered vertical surface displacement amplitude due to a Rayleigh wave propagating in the x-direction. H = depth of cavity center = $2.6A$, $k_2A = 0.6$.

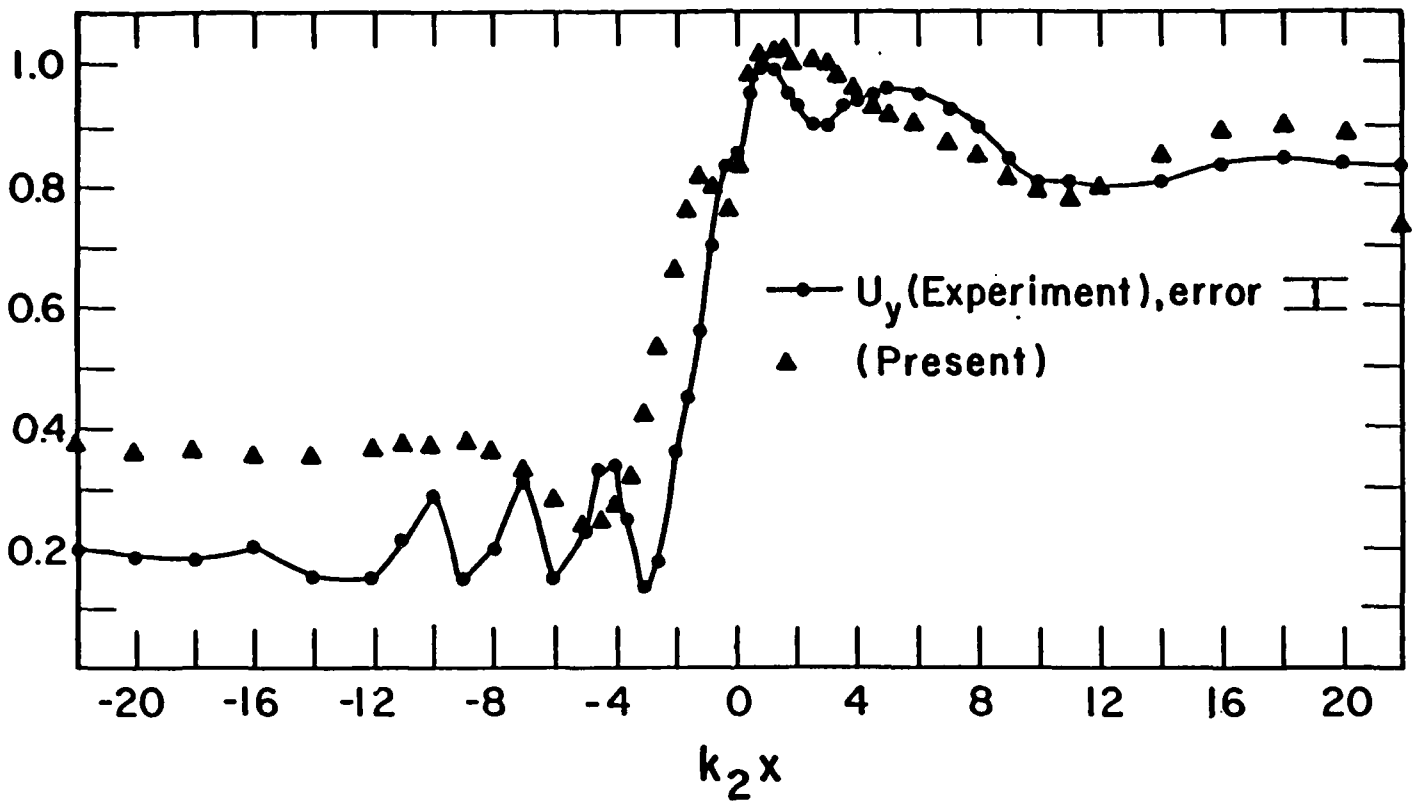

FIGURE 8. *Scattered vertical surface displacement amplitude due to a Rayleigh wave incident on a buried inclusion. Properties of inclusion and matrix are, respectively,* $c_1' = 5.18km/s$, $c_2' = 2.87km/s$, $c_1 = 6.4km/s$, $c_2 = 3.13km/s$. $H/A = 1.53$.

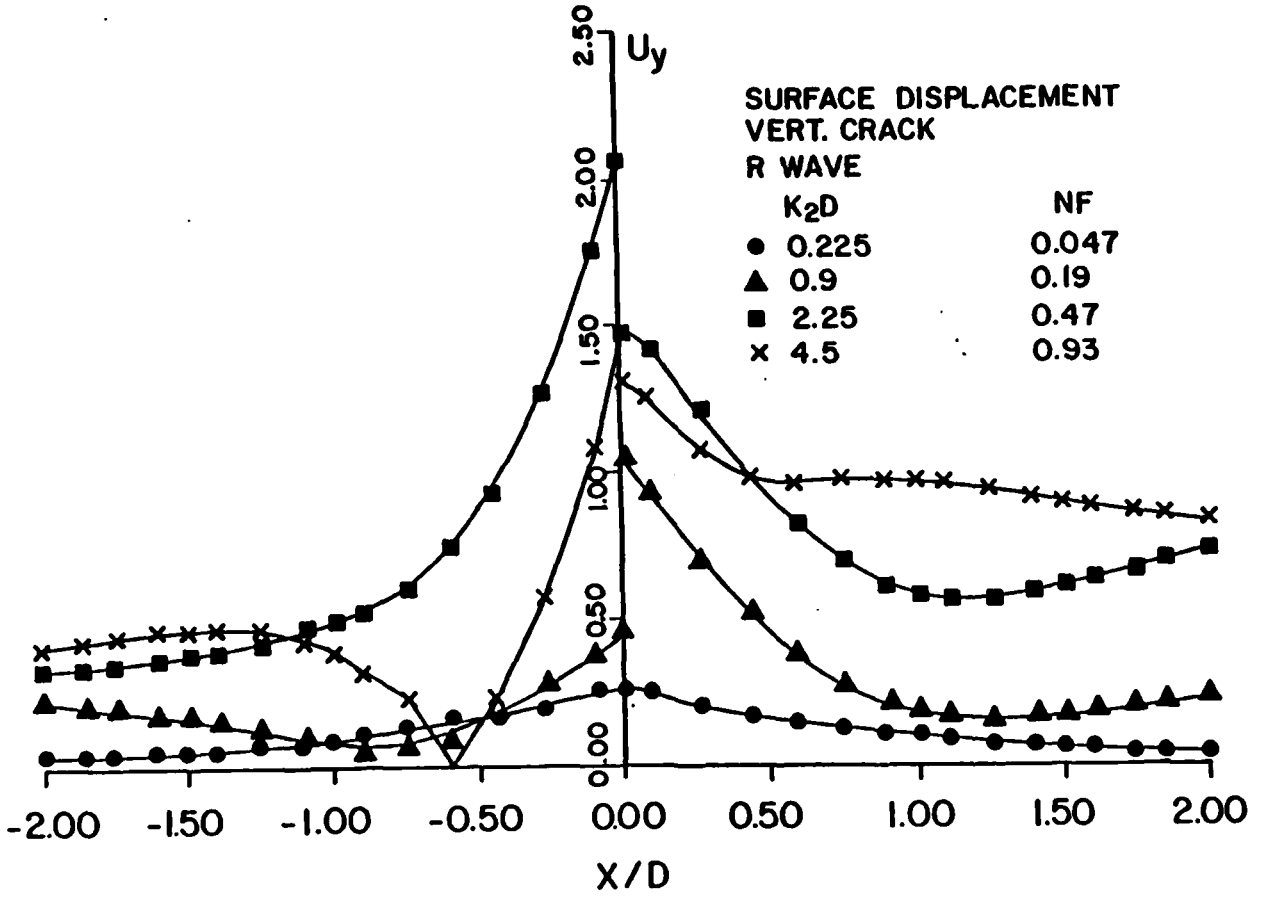

FIGURE 9. Scattered vertical surface displacement amplitude for a normal surface-breaking planar crack.

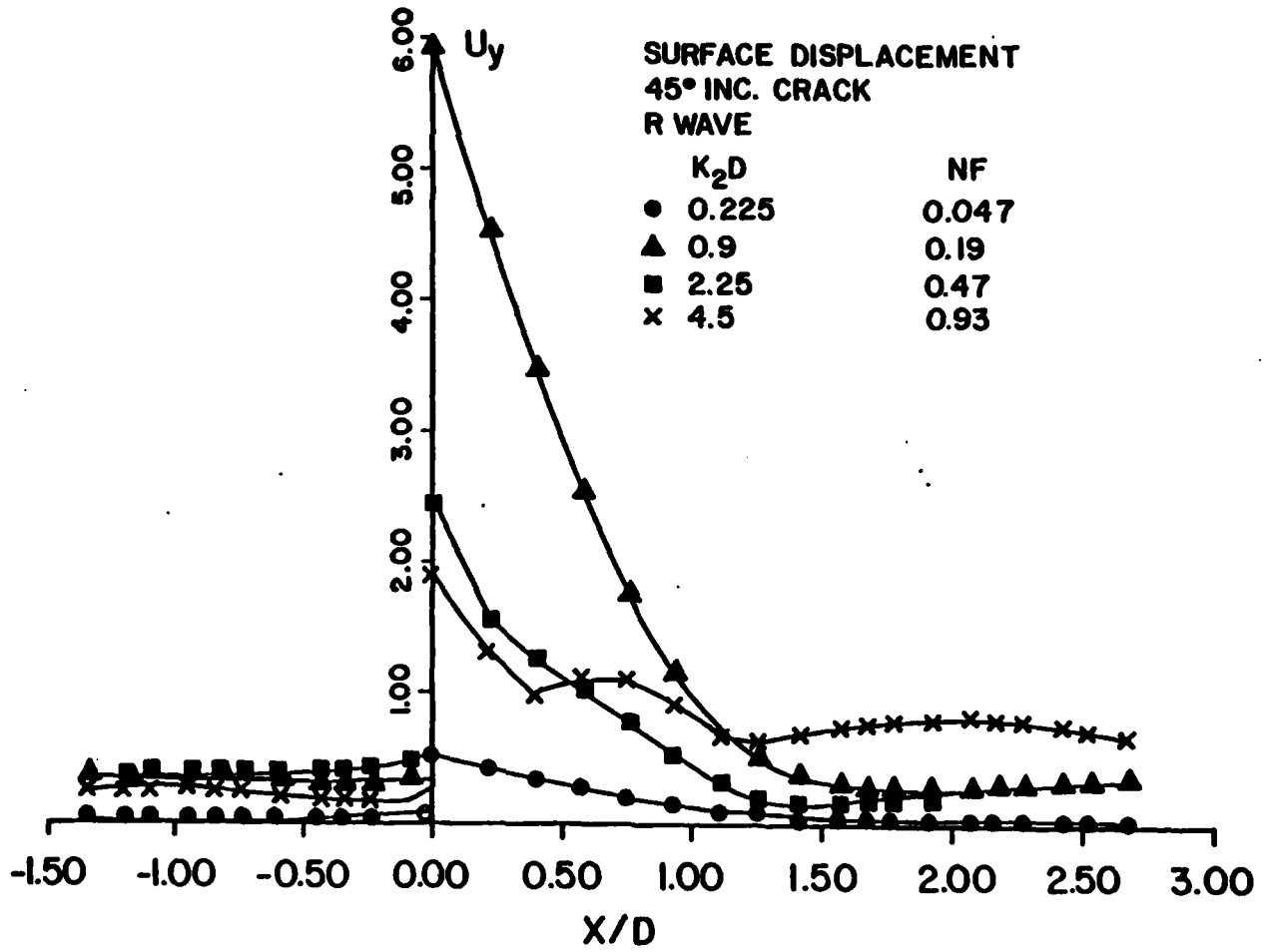

FIGURE 10. Scattered vertical surface displacement amplitude due to a canted surface-breaking planar crack.

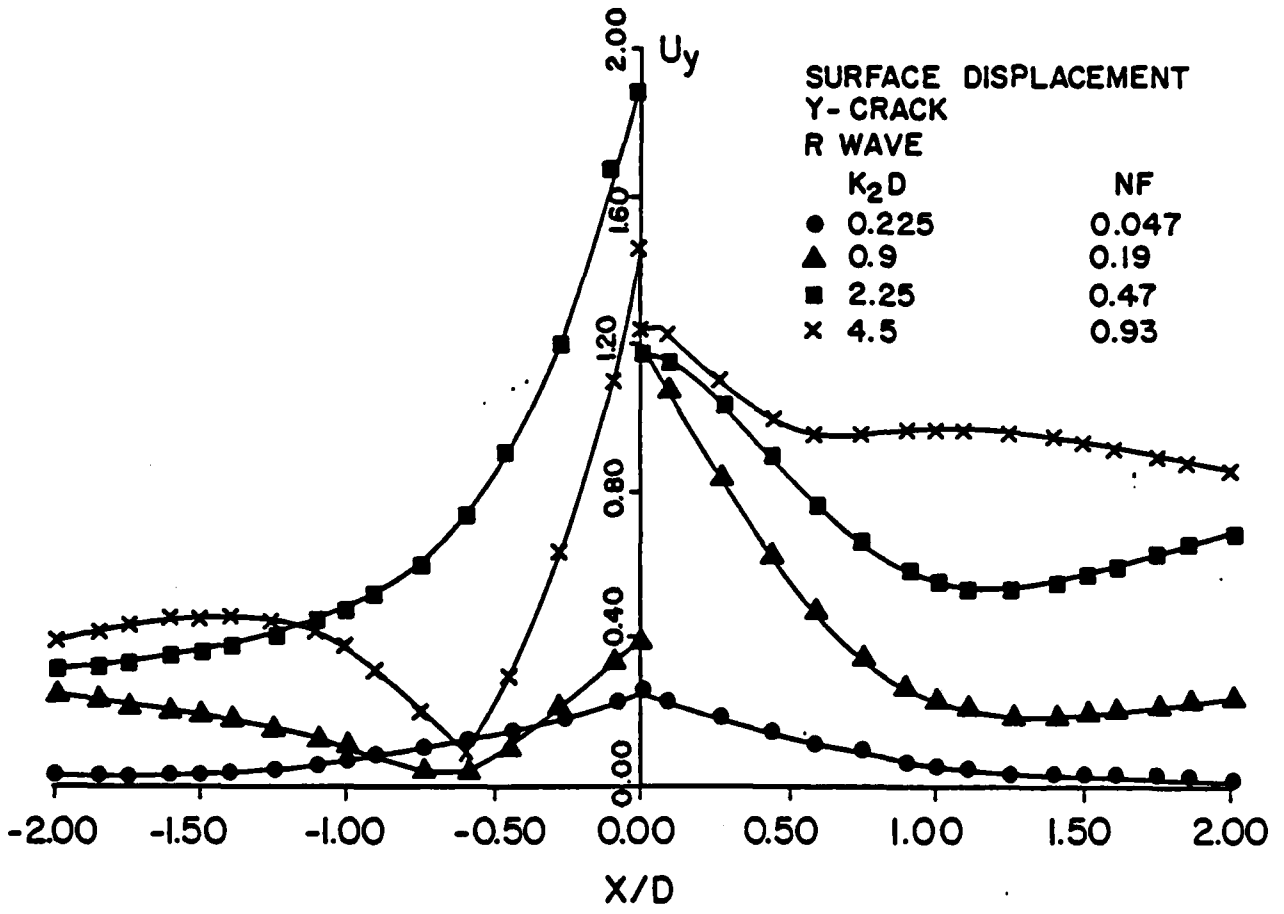

FIGURE 11. Scattered vertical surface displacement amplitude due to a normal branched surface-breaking crack.

CONCLUSION

Results presented above show the versatility and success of the hybrid modeling technique to solve ultrasonic scattering by single or multiple defects in unbounded and bounded media. Comparison of theoretical and experimental results shows excellent agreement. These studies show that the hybrid modeling technique is capable of describing the scattering process in a variety of situations that involve more than one defect and non-planar defects.

The analysis that has been presented above for a homogeneous isotropic plate can be extended to layered and anisotropic plates modeling laminated composites. That work is in progress and will be reported later.

ACKNOWLEDGMENTS

The works reported here were supported partly by grants from the National Science Foundation (CEE-8120536), Office of Naval Research (N00014-86-K-0280), and Natural Science and Engineering Research Council of Canada (A-7988).

REFERENCES

1. M.G. Silk, "Defect detection and sizing in metals using ultra-sound," *International Metals Review*, Vol. 27, 1982, pp. 28-50.

2. V. Varatharajulu and Y.H. Pao, "Scattering matrix for elastic waves, I. Theory," *Journal of the Acoustical Society of America*, Vol. 60, 1976, pp. 556-566.

3. A.H. Shah, K.C. Wong, and S.K. Datta, "Single and multiple scattering of elastic waves in two dimensions," *Journal of the Acoustical Society of America*, Vol. 74, 1983, pp. 1033-1043.

4. Z.S. Abduljabbar, S.K. Datta and A.H. Shah, "Diffraction of horizontally polarized shear waves by normal edge cracks in a plate," *Journal of Applied Physics*, Vol. 54, 1983, pp. 461-472.

5. A.H. Shah, K.C. Wong and S.K. Datta, "Surface displacements due to elastic wave scattering by buried planar and non-planar cracks," *Wave Motion*, Vol. 7, 1985, pp. 319-333.

6. S.K. Datta, K.C. Wong, and A.H. Shah, "Dynamic stresses and displacements around cylindrical cavities of arbitrary shape," *Journal of Applied Mechanics*, Vol. 51, 1984, pp. 798-803.

7. K.C. Wong, A.H. Shah and S.K Datta, "Diffraction of elastic waves in a half-space. II. Analytical and numerical solutions," *Bulletin of the Seismological Society of America*, Vol. 75, 1985, pp. 69-92.

8. A.H. Shah, K.C. Wong and S.K. Datta, "Diffraction of SH waves in a half-space," *Earthquake Engineering and Structural Dynamics*, Vol. 10, 1982, pp. 519-528.

9. S.K. Datta, A.H. Shah and C.M. Fortunko, "Diffraction of medium and long wavelength horizontally polarized shear waves by edge cracks," *Journal of Applied Physics*, Vol. 53, pp. 2895-2903.

10. Z.S. Abduljabbar, *Diffraction of Horizontally Polarized Shear Waves by Cracks in a Thick Plate*, Ph.D. Thesis, University of Colorado, Boulder, Colorado, 1983.

11. S.K. Datta and A.H. Shah, "Diffraction of horizontally polarized shear waves," *Numerical Methods in Engineering*, Vol. 2, Pluralis, Paris, 1983.

12. S.K. Datta, R.E. Schramm and Z. Abduljabbar, "Plate Modes Generated by EMATs for NDE of Planar Flaws," *Review of Progress in Quantitative Nondestructive Evaluation*, to be published.

13. S.K. Datta and N. El-Akily, "Diffraction of elastic waves by cylindrical cavity in a half-space," *Journal of the Acoustical Society of America*, Vol. 64, 1978, pp. 1692-1699.

14. A.H. Shah, Y.F. Chin and S.K. Datta, "Elastic Wave Scattering by Surface-breaking Planar and Non-planar Cracks," to be published.

END

11-86

DTIC